Non-linear BFKL dynamics:
color screening vs. gluon fusion

R. Fiore[1], *P. V. Sasorov*[+ 1], *V. R. Zoller*[+ 1]

Dipartimento di Fisica, Università della Calabria

Istituto Nazionale di Fisica Nucleare, Gruppo collegato di Cosenza,
I-87036 Rende, Cosenza, Italy

[+] *Alikhanov Institute for Theoretical and Experimental Physics, 117218 Moscow, Russia*

A feasible mechanism of unitarization of amplitudes of deep inelastic scattering at small values of Bjorken x is the gluon fusion. However, its efficiency depends crucially on the vacuum color screening effect which accompanies the multiplication and the diffusion of BFKL gluons from small to large distances. From the fits to lattice data on field strength correlators the propagation length of perturbative gluons is $R_c \simeq (0.2-0.3)$ Fm. The probability to find a perturbative gluon with short propagation length at large distances is suppressed exponentially. It changes the pattern of (dif)fusion dramatically. The magnitude of the fusion effect appears to be controlled by the new dimensionless parameter $\sim R_c^2/8B$, with the diffraction cone slope B standing for the characteristic size of the interaction region. It should slowly $\propto 1/\ln Q^2$ decrease at large Q^2. Smallness of the ratio $R_c^2/8B$ makes the non-linear effects rather weak even at lowest Bjorken x available at HERA. We report the results of our studies of the non-linear BFKL equation which has been generalized to incorporate the running coupling and the screening radius R_c as the infrared regulator.

1. Introduction.
In processes of deep inelastic scattering (DIS) the density of BFKL [1] gluons, $\mathcal{F}(x, k^2)$, grows fast to smaller values of Bjorken x, $\mathcal{F}(x, k^2) \propto x^{-\Delta}$, where, phenomenologically, $\Delta \approx 0.3$. The growth of $\mathcal{F}(x, k^2)$ will have to slow down when the gluon densities become large enough that fusion processes $gg \to g$ become important. It was the original parton model idea of Refs. [2, 3] developed further within QCD in [4, 5]. The BFKL dynamics of saturation of the parton densities has been discussed first in [6–8], for the alternative form of the fusion correction see Eq. (A10) of Ref. [9]. The literature abounds with suggestions of different versions of the non-linear evolution equation, see e.g. [10].

There is, however, at least one more mechanism to prevent generation of the high density gluon states. This is well known the vacuum color screening. The non-perturbative fluctuations in the QCD vacuum restrict the phase space for the perturbative (real and virtual) gluons introducing a new scale: the correlation/propagation radius R_c of perturbative gluons. The perturbative gluons with short propagation length, $R_c \sim \sim (0.2-0.3)$ Fm, as it follows from the fits to lattice data on field strength correlators [11], do not walk to large distances, where they supposedly fuse together. The fusion probability decreases. We show that it is controlled

by the new dimensionless parameter $R_c^2/8B$, with the diffraction cone slope B standing for the characteristic size of the region populated with interacting gluons.

The effects of finite R_c are consistently incorporated by the generalized color dipole (CD) BFKL equation (hereafter CD BFKL) [12, 13]. In presence of a new scale the saturation phenomenon acquires some new features and the goal of this communication is to present their quantitative analysis.

2. CD BFKL and phenomenology of DIS.
We sketch first the CD BFKL equation for $q\bar{q}$ dipole-nucleon cross section $\sigma(\xi, r)$, where $\xi = \ln(x_0/x)$ and r is the $q\bar{q}$-separation. The BFKL cross section $\sigma(\xi, r)$ sums the Leading-log$(1/x)$ multi-gluon production cross sections within the QCD perturbation theory (PT). Consequently, as a realistic boundary condition for the BFKL dynamics one can take the lowest PT order $q\bar{q}$-nucleon cross section at some $x = x_0$. It is described by the Yukawa screened two-gluon exchange

$$\sigma(0,r) \equiv \sigma_0(r) = 4C_F \int \frac{d^2\mathbf{k}}{(k^2 + \mu_G^2)^2} \alpha_S(k^2)\alpha_S(\kappa^2) \times$$
$$\times [1 - J_0(kr)][1 - F_2(\mathbf{k}, -\mathbf{k})], \quad (1)$$

where $\mu_G = 1/R_c$, $\alpha_S(\kappa^2) = 4\pi/\beta_0 \ln(\kappa^2/\Lambda_{\text{QCD}}^2)$ and $\kappa^2 = \max\{k^2, C^2/r^2\}$. The two-quark form factor of the nucleon can be related to the single-quark form factor

$$F_2(\mathbf{k}, -\mathbf{k}) = F_1(uk^2). \quad (2)$$

[1] e-mail: roberto.fiore@cs.infn.it; sasorov@itep.ru; zoller@itep.ru

The latter is close to the charge form factor of the proton $F_1(q^2) \approx F_p(q^2) = 1/(1 + q^2/\Lambda^2)^2$, where $\Lambda^2 = 0.71$ GeV^2 and in Eq. (2) $u = 2N_c/(N_c - 1)$ for the color group SU(N_c) [14].

The small-x evolution correction to $\sigma(\xi, r)$ for the perturbative 3-parton state $q\bar{q}g$ is as follows [12, 13]

$$\partial_\xi \sigma(\xi, r) = \int d^2\boldsymbol{\rho}_1 \, |\psi(\boldsymbol{\rho}_1) - \psi(\boldsymbol{\rho}_2)|^2 \times$$
$$\times [\sigma_3(\xi, \mathbf{r}, \boldsymbol{\rho}_1, \boldsymbol{\rho}_2) - \sigma(\xi, r)], \quad (3)$$

where the 3-parton ($q\bar{q}g$-nucleon) cross section is

$$\sigma_3(\xi, \mathbf{r}, \boldsymbol{\rho}_1, \boldsymbol{\rho}_2) =$$
$$= \frac{C_A}{2C_F} [\sigma(\xi, \rho_1) + \sigma(\xi, \rho_2) - \sigma(\xi, r)] + \sigma(\xi, r), \quad (4)$$

where $C_A = N_c$ and $C_F = (N_c^2 - 1)/2N_c$. Denoted by $\boldsymbol{\rho}_{1,2}$ are the q-g and $\bar{q}$-g separations in the two-dimensional impact parameter plane for dipoles generated by the $\bar{q}$-q color dipole source. The radial light cone wave function $\psi(\boldsymbol{\rho})$ of the dipole with the vacuum screening of infrared gluons is [12, 13]

$$\psi(\boldsymbol{\rho}) = \frac{\sqrt{C_F \alpha_S(R_i)}}{\pi} \frac{\boldsymbol{\rho}}{\rho R_c} K_1(\rho/R_c), \quad (5)$$

where $K_\nu(x)$ is the modified Bessel function. The one-loop QCD coupling

$$\alpha_S(R_i) = 4\pi/\beta_0 \ln(C^2/\Lambda_{\text{QCD}}^2 R_i^2) \quad (6)$$

is taken at the shortest relevant distance $R_i = \min\{r, \rho_i\}$. In the numerical analysis $C = 1.5$, $\Lambda_{\text{QCD}} = 0.3\,\text{GeV}$, $\beta_0 = (11N_c - 2N_f)/3$, and infrared freezing $\alpha_S(r > r_f) = \alpha_f = 0.8$ has been imposed (for more discussion see [15]). The scaling BFKL equation [1] is obtained from Eq. (3) at $r, \rho_{1,2} \ll R_c$ in the approximation $\alpha_S = \text{const}$ – the dipole picture suggested in [16].

3. Perturbative and non-perturbative. The perturbative gluons are confined and do not propagate to large distances. Available fits [11] to the lattice QCD data suggest Yukawa screening of perturbative color fields with propagation/screening radius $R_c \approx (0.2-0.3)\,\text{Fm}$. The value $R_c = 0.275\,\text{Fm}$ has been used since 1994 in the very successful color dipole phenomenology of small-x DIS [17–21]. Because the propagation radius is short compared to the typical range of strong interactions the dipole cross section obtained as a solution of the CD BFKL equation (3) would miss the interaction strength for large color dipoles. In [17, 18] this missing strength was modeled by the x-independent dipole cross section and it has been assumed that the per-

turbative, $\sigma(\xi, r)$, and non-perturbative, $\sigma_{\text{npt}}(r)$, cross sections are additive,

$$\sigma_{\text{tot}}(\xi, r) = \sigma(\xi, r) + \sigma_{\text{npt}}(r). \quad (7)$$

The principal point about the non-perturbative component of $\sigma_{\text{tot}}(\xi, r)$ is that it must not be subjected to the perturbative BFKL evolution. Thus, the arguments about the rise of $\sigma(\xi, r)$ due to the hard-to-soft diffusion do not apply to $\sigma_{\text{npt}}(r)$. We reiterate, finite R_c means that gluons with the wave length $\lambda \gtrsim R_c$ are beyond the realm of perturbative QCD. A quite common application of purely perturbative non-linear equations [6, 7] to the analysis of DIS data without proper separation of perturbative and non-perturbative contributions is completely unwarranted.

Specific form of $\sigma_{\text{npt}}(r)$ motivated by the QCD string picture and used in the present paper is as follows:

$$\sigma_{\text{npt}}(r) = a\alpha_S^2(r)r^2/(r + d). \quad (8)$$

Here $d = 0.5\,\text{Fm}$ is close to the radius of freezing of the running QCD coupling r_f and $a = 5\,\text{Fm}$.

Our choice $R_c = 0.26\,\text{Fm}$ leads to a very good description of the data [22–26] on the proton structure function $F_2(x, Q^2)$ at small x shown in Fig. 1. Shown separately are the nonperturbative contribution (8) and the contribution from DIS off valence quarks [27]. The effects of quark masses important at low Q^2 are taken into account [28]. The linear CD BFKL description of $F_2(x, Q^2)$ (dashed line) is perfect at moderate and high Q^2, where it is indistinguishable from the solid line representing the non-linear CD BFKL results (see below). Two lines diverge at low Q^2 where the account of the non-linear effects improves the agreement with data.

Recently a global analysis of HERA DIS data has been reported [29]. In [29] a purely perturbative non-linear equation is solved with some phenomenological initial conditions. A very soft infrared regularization with the infrared cutoff $\sim \Lambda_{\text{QCD}}^{-1}$ allows non-perturbatively large dipoles to be governed by the perturbative QCD dynamics. The non-perturbative component of solution evolves perturbatively to smaller x. Good agreement with data was found.

4. CD BFKL and the partial-wave amplitudes. Following [30, 31] we rewrite the Eq. (3) in terms of the $q\bar{q}$-nucleon partial-wave amplitudes (profile functions) $\Gamma(\xi, \mathbf{r}, \mathbf{b}) = 1 - S(\xi, \mathbf{r}, \mathbf{b})$ related to the scattering matrix $S(\xi, \mathbf{r}, \mathbf{b})$. We introduce the impact parameter $\mathbf{b}$ defined with respect to the center of the q-$\bar{q}$ dipole. In the $q\bar{q}g$ state, the qg and $\bar{q}g$ dipoles have the impact parameter $\mathbf{b} + \boldsymbol{\rho}_{2,1}/2$. In the large-$N_c$ approximation σ_3 in Eq. (4)
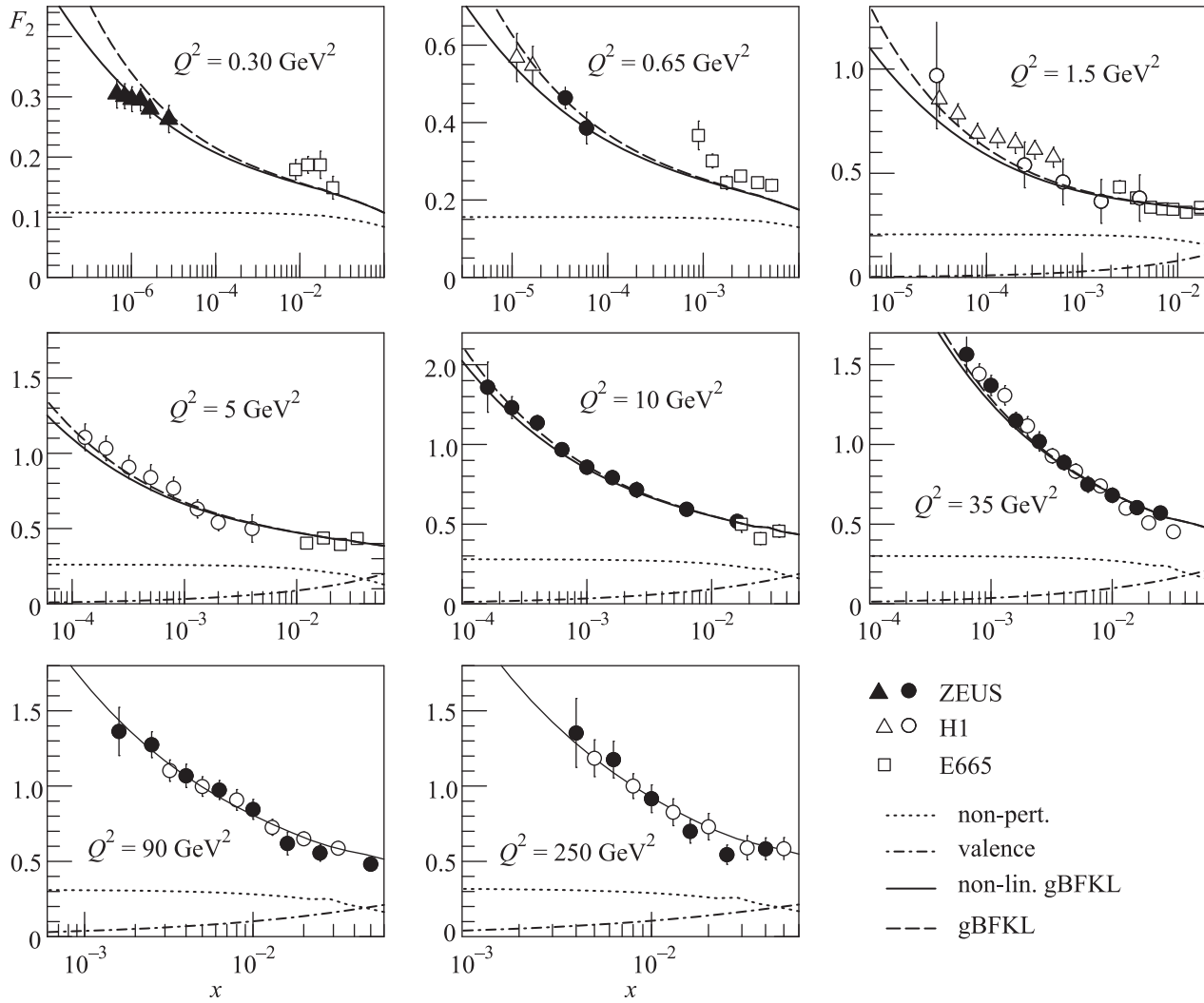
Fig. 1. The CD BFKL description of the experimental data on $F_2(x, Q^2)$. Black triangles and circles are ZEUS data [22, 23], open triangles and circles show H1 data [24, 25] and open squares refer to E665 results [26]. Dashed lines represent the linear CD BFKL structure function F_2. Shown by solid lines are the non-linear CD BFKL structure functions F_2. At high Q^2 the non-linear effects vanish and both dashed and solid lines are indistinguishable. The valence and non-perturbative corrections are included into both the CD BFKL and the non-linear CD BFKL description of F_2. The contribution to F_2 from DIS off valence quarks [27] is shown separately by dash-dotted lines. Shown by dotted lines are the non-perturbative contributions to F_2

reduces to $\sigma_3 = \sigma(\xi, \boldsymbol{\rho}_1) + \sigma(\xi, \boldsymbol{\rho}_2)$, what corresponds to the factorization of the 3-parton ($q\bar{q}g$) scattering matrix,

$$S_3(\xi, \mathbf{r}, \boldsymbol{\rho}_1, \boldsymbol{\rho}_2) = S\left(\xi, \rho_1, \mathbf{b} + \frac{1}{2}\boldsymbol{\rho}_2\right) S\left(\xi, \rho_2, \mathbf{b} + \frac{1}{2}\boldsymbol{\rho}_1\right).$$
(9)

Then, the renormalization of the $q\bar{q}$-nucleon scattering matrix, $S(\xi, \mathbf{r}, \mathbf{b})$, for the perturbative 3-parton state $q\bar{q}g$ is as follows

$$\partial_\xi S(\xi, r, \mathbf{b}) = \int d^2\boldsymbol{\rho}_1 \ |\psi(\boldsymbol{\rho}_1) - \psi(\boldsymbol{\rho}_2)|^2 \times$$
(10)

$$\times \left[S\left(\xi, \rho_1, \mathbf{b} + \frac{1}{2}\boldsymbol{\rho}_2\right) S\left(\xi, \rho_2, \mathbf{b} + \frac{1}{2}\boldsymbol{\rho}_1\right) - S(\xi, r, \mathbf{b}) \right].$$

For the early discussion of Eq. (10) see [6, 7]. The substitution $S(\xi, \mathbf{r}, \mathbf{b}) = 1 - \Gamma(\xi, \mathbf{r}, \mathbf{b})$ results in

$$\partial_\xi \Gamma(\xi, r, \mathbf{b}) = \int d^2\boldsymbol{\rho}_1 \ |\psi(\boldsymbol{\rho}_1) - \psi(\boldsymbol{\rho}_2)|^2 \times$$

$$\times \left[\Gamma\left(\xi, \rho_1, \mathbf{b} + \frac{1}{2}\boldsymbol{\rho}_2\right) + \right.$$

$$+ \Gamma\left(\xi, \rho_2, \mathbf{b} + \frac{1}{2}\boldsymbol{\rho}_1\right) - \Gamma(\xi, r, \mathbf{b}) \right] -$$

$$- \Gamma\left(\xi, \rho_2, \mathbf{b} + \frac{1}{2}\boldsymbol{\rho}_1\right) \Gamma\left(\xi, \rho_1, \mathbf{b} + \frac{1}{2}\boldsymbol{\rho}_2\right).$$
(11)

We identify the corresponding partial waves using the conventional impact parameter representation for the elastic dipole-nucleon amplitude

$$f(\xi, r, \mathbf{k}) = 2 \int d^2\mathbf{b} \exp(-i\mathbf{b}\mathbf{k}) \Gamma(\xi, r, \mathbf{b}). \qquad (12)$$

For the predominantly imaginary $f(\xi, r, \mathbf{k}) = i\sigma(\xi, r) \exp(-Bk^2/2)$ the profile function is

$$\Gamma(\xi, r, \mathbf{b}) = \frac{\sigma(\xi, r)}{4\pi B(\xi, r)} \exp\left[-\frac{b^2}{2B(\xi, r)}\right], \qquad (13)$$

and $\sigma(\xi, r) = 2 \int d^2\mathbf{b}\Gamma(\xi, r, \mathbf{b})$.

Integrating over $\mathbf{b}$ Eq. (11) yields [32]

$$\partial_\xi \sigma(\xi, r) = \int d^2\boldsymbol{\rho}_1 |\psi(\boldsymbol{\rho}_1) - \psi(\boldsymbol{\rho}_2)|^2 \times$$
$$\times \left\{ \sigma(\xi, \rho_1) + \sigma(\xi, \rho_2) - \sigma(\xi, r) - \right.$$
$$\left. - \frac{\sigma(\xi, \rho_1)\sigma(\xi, \rho_2)}{4\pi(B_1 + B_2)} \exp\left[-\frac{r^2}{8(B_1 + B_2)}\right] \right\}, \qquad (14)$$

where $B_i = B(\xi, \rho_i)$. The above definition of the scattering profile function, Eq. (13), removes uncertainties with the radius R of the area within which interacting gluons are expected to be distributed (the parameter $S_\perp = \pi R^2$ appearing in Eq. (25)). In different analyses of the non-linear effects its value varies from the realistic $R^2 = 16\,\text{GeV}^{-2}$ [33] down to the intriguing small $R^2 = 3.1\,\text{GeV}^{-2}$ [34]. Besides, the radius R is usually assumed to be independent of x. In our approach the area populated with interacting gluons is proportional to the diffraction cone slope $B(\xi, r)$.

5. The diffraction cone slope. The diffraction slope for the forward cone in the dipole-nucleon scattering [30] was presented in [31] in a very symmetric form

$$B(\xi, r) = \frac{1}{2}\langle\mathbf{b}^2\rangle = \frac{1}{8}r^2 + \frac{1}{3}R_N^2 + 2\alpha'_{\mathbf{IP}}\xi. \qquad (15)$$

The latter provides the beam, target and exchange decomposition of B: $r^2/8$ is the purely geometrical term for the color dipole of the size r, R_N represents the gluon-probed radius of the proton, the dynamical component of B is given by the last term in Eq. (15), where $\alpha'_{\mathbf{IP}}$ is the Pomeron trajectory slope evaluated first in [30] (see also [31]). The order of magnitude estimate [31]

$$\alpha'_{\mathbf{IP}} \sim \frac{3}{16\pi^2} \int d^2\mathbf{r}\alpha_S(r)R_c^{-2}r^2 K_1^2(r/R_c) \sim$$
$$\sim \frac{3}{16\pi}\alpha_S(R_c)R_c^2, \qquad (16)$$

clearly shows the connection between the dimensionful $\alpha'_{\mathbf{IP}}$ and the non-perturbative infrared parameter R_c.

The increase of B with growing collision energy is known as the phenomenon of shrinkage of the diffraction cone.

We determine $\alpha'_{\mathbf{IP}}$ as the $\xi \to \infty$ limit of the local Regge slope $\alpha'_{\text{eff}}(\xi, r) = \partial_\xi B(\xi, r)/2$ [31]. At $\xi \to \infty$, $\alpha'_{\text{eff}}(\xi, r)$ tends to a r-independent $\alpha'_{\mathbf{IP}} = 0.064\,\text{GeV}^{-2}$. The onset of the limiting value $\alpha'_{\mathbf{IP}}$ is very slow and correlates nicely with the very slow onset of the BFKL asymptotics of $\sigma(\xi, r)$ [12]. An interesting finding of Ref. [31] is a large sub-asymptotic value of the effective Regge slope $\alpha'_{\text{eff}}(\xi, r)$, which is by the factor $\sim 2-3$ larger than $\alpha'_{\mathbf{IP}}$.

In Eq. (15) the gluon-probed radius of the proton is a phenomenological parameter to be determined from the experiment. The analysis of Ref. [35] gives $R_N^2 \approx \approx 12\,\text{GeV}^{-2}$.

6. Non-linear CD BFKL: small dipoles, $r \ll R_c$. The term quadratic in σ in Eq. (14), models the process of the gluon fusion. The efficiency of this "fuser" differs substantially for $r \ll R_c$ and for $r \gtrsim R_c$. Consider first the ordering of dipole sizes

$$r^2 \ll \rho^2 \ll R_c^2 \qquad (17)$$

corresponding to the Double Leading Log Approximation (DLLA) [36]. Eq. (14) reduces to

$$\partial_\xi \sigma(\xi, r) = \frac{C_F}{\pi}\alpha_S(r)r^2 \times$$
$$\times \int_{r^2}^{R_c^2} \frac{d\rho^2}{\rho^4}\left[2\sigma(\xi, \rho) - \frac{\sigma(\xi, \rho)^2}{8\pi B}\right]. \qquad (18)$$

First notice that the function

$$g(\xi, \rho) = \rho^{-2}\sigma(\xi, \rho) \qquad (19)$$

is essentially flat in ρ and the second term in the *rhs* of Eq. (18) is dominated by $\rho \sim R_c$,

$$\frac{1}{8B}\int_{r^2}^{R_c^2} \frac{d\rho^2}{\rho^4}\sigma(\xi, \rho)^2 \simeq \frac{R_c^2}{8B}g(\xi, R_c)^2 \qquad (20)$$

with $B = B(\xi, R_c)$. Thus, the new dimensionless parameter

$$\kappa_c = R_c^2/8B \qquad (21)$$

enters the game. Its geometrical meaning is quite clear. Remind that the unitarity requires (see Eq. (13))

$$\sigma(\xi, \rho) \le 8\pi B. \qquad (22)$$

Smallness of κ_c makes the non-linear effects rather weak at HERA even at lowest available Bjorken x (see Fig. 1). Comparison of the linear and quadratic terms

in the right hand side of Eq. (18) shows that the relative strength of non-linear effects decreases to smaller $r^2 \sim Q^{-2}$ logarithmically

$$\kappa = \frac{\text{quadr.}}{\text{lin.}} \propto \kappa_c \ln^{-1}(Q^2 R_c^2). \qquad (23)$$

Therefore, we are dealing with the scaling rather than the higher twist, $1/Q^2$, effect.

7. Saturation scale and observables. The parameter κ in Eq. (23) should not be confused with another parameter frequently used to quantify the strength of the non-linear effects. It decreases with growing Q^2 much faster than κ in Eq. (23). Namely,

$$\kappa \sim 1/Q^2. \qquad (24)$$

The estimate (24) comes from equating the linear and non-linear terms in *rhs* of the equation [4, 5]

$$\partial_\xi \partial_\eta G(\xi, \eta) = c G(\xi, \eta) - \frac{a}{Q^2} G(\xi, \eta)^2, \qquad (25)$$

where $\eta = \ln(Q^2/\Lambda_{\text{QCD}}^2)$, $c = \alpha_S N_c/\pi$, $a = \alpha_S^2 \pi/S_\perp$, $G(\xi, \eta)$ is the integrated gluon density and Eq. (25) comes from Eq. (18) as for small dipoles $g(\xi, \rho) \approx$ $\approx \frac{\pi^2}{N_c} \alpha_S(\rho) G(\xi, \rho)$. The corresponding value of Q^2 denoted by

$$Q_s^2 = a G(x, Q_s^2)/c \qquad (26)$$

is called the saturation scale. The non-linear saturation effects are assumed to be substantial for all $Q \lesssim Q_s$ (see e.g. [37]). Obviously, Eq. (23) asserts something different. The point is that Eqs. (23) and (24) describe the Q^2-dependence of strength of the non-linear effects for two very different quantities: the integrated gluon density $G(\xi, \eta)$ and the differential gluon density $\mathcal{F}(\xi, \eta) = \partial_\eta G(\xi, \eta)$, respectively. The gluon density $G(\xi, \eta)$ is a directly measurable quantity. For example, the longitudinal DIS structure function is $F_L(x, Q^2) \sim$ $\sim \alpha_S(Q^2) G(x, Q^2)$ [38]. On the contrary, the differential gluon density $\mathcal{F}(\xi, \eta)$ is related to the observable quantities like $F_2(x, Q^2)$ rather indirectly, by means of the well known transformations leaving a weak trace of Eq. (24) in $F_2(x, Q^2)$.

A possibility to test Eqs. (24) and (26) provides the coherent diffractive dijet production in pion-nucleon and pion-nucleus collisions [39]. Both helicity amplitudes of the process are directly proportional to $\mathcal{F}(x, k^2)$. The same proportionality of diffractive amplitudes to $\mathcal{F}(x, k^2)$ was found for real photoproduction with point-like $\gamma q\bar{q}$ vertex in [40]. Therefore, there is no real clash between Eqs. (23) and (24). The sharp Q^2-dependence

of the nonlinear term in Eq. (25) does not imply vanishing non-linear effects in $G(x, Q^2)$ for $Q^2 \gg Q_s^2$.

8. Non-linear CD BFKL: large dipoles, $r \gtrsim R_c$. The interplay of the color screening and gluon fusion effects at large $r \gtrsim R_c$, where the non-linear effects are expected to be most pronounced, requires special investigation. In high-energy scattering of large quark-antiquark dipoles, $r \gg R_c$, a sort of the additive quark model is recovered: the (anti)quark of the dipole r develops its own perturbative gluonic cloud and the pattern of diffusion changes dramatically. Indeed, in this region the term proportional to $K_1(\rho_1/R_c) K_1(\rho_2/R_c)$ in the kernel of Eq. (3) is exponentially small, what is related to the exponential decay of the correlation function (the propagator) of perturbative gluons. Then, at large r the kernel will be dominated by the contributions from $\rho_1 \lesssim R_c \ll \rho_2 \simeq r$ and from $\rho_2 \lesssim R_c \ll \rho_1 \simeq r$. It does not depend on r and for large N_c the equation for the dipole cross section reads

$$\partial_\xi \sigma(\xi, r) = \frac{\alpha_S C_F}{\pi^2} \int d^2\rho_1 R_c^{-2} K_1^2(\rho_1/R_c) \times$$
$$\times \left\{ \sigma(\xi, \rho_1) + \sigma(\xi, \rho_2) - \sigma(\xi, r) - \right.$$
$$\left. - \frac{\sigma(\xi, \rho_1) \sigma(\xi, \rho_2)}{4\pi(B_1 + B_2)} \exp\left[-\frac{r^2}{8(B_1 + B_2)}\right] \right\}, \qquad (27)$$

where $B_i = B(\xi, \rho_i)$. For a qualitative understanding of the role of color screening in the non-linear dynamics of large dipoles we reduce Eq. (27) to the differential equation. First notice that the dipole cross section $\sigma(\xi, r)$ as a function of r varies slowly in the region $r \gg R_c$, while the function $K_1(y)$ vanishes exponentially at $y \gg 1$ and $K_1(y) \approx 1/y$ for $y \ll 1$. Therefore, Eq. (27) can be cast in the following form

$$c^{-1} \partial_\xi \sigma(\xi, r) = \sigma(\xi, R_c) + R_c^2 \partial_{r^2} \sigma(\xi, r) - $$
$$- \sigma(\xi, R_c) \sigma(\xi, r)/8\pi B, \qquad (28)$$

where $c = \alpha_S C_F/\pi$ and for simplicity $B = B(0, R_c)$. The solution of Eq. (28) with the boundary condition $\sigma(0, r) = \sigma_0(r^2)$, where $\sigma_0(r^2)$ comes from Eq. (1), is

$$\sigma(\xi, r) = \frac{\sigma_0(r^2 + c\xi R_c^2) + v(\xi)}{1 + v(\xi)/8\pi B}, \qquad (29)$$

where

$$v(\xi) = e^{c\xi} \int_0^{c\xi} \sigma_0(R_c^2 + z R_c^2) e^{-z} dz. \qquad (30)$$

From Eq. (1) it follows that at $r \ll l = $ $= \min\{R_c/\sqrt{2}, \sqrt{u}/\Lambda\}$

$$\sigma_0(r^2) \approx \frac{4\pi^2 C_F}{\beta_0} r^2 \alpha_S(r/\sqrt{A}) \ln\frac{\alpha_S(l)}{\alpha_S(r/\sqrt{A})}, \qquad (31)$$

where $A \approx 10$ comes from properties of the Bessel function $J_0(y)$ in Eq. (1) [41]. For large dipoles $\sigma_0(r^2)$ saturates at $r^2 \simeq Al^2$,

$$\sigma_0(r^2) \approx 4\pi C_F R_c^2 \alpha_f \alpha_S(R_c) h(a), \qquad (32)$$

where $\alpha_f = 0.8$ (see Eq. (6)) and the interplay of two scales, R_c and Λ^{-1}, in Eq. (1) results in $h(a) = 1 - (a^2 - 1 - 2a \ln a)/(a-1)^3$ with $a = u/R_c^2\Lambda^2$. This kind of saturation is due to the finite propagation radius of perturbative gluons.

With growing ξ the dipole cross section $\sigma(\xi, r)$ increases approaching the unitarity bound, $\sigma = 8\pi B$. To quantify the strength of the non-linear effects we introduce the parameter

$$\kappa = \delta\sigma/\sigma, \qquad (33)$$

where $\delta\sigma = \sigma - \sigma_{nl}$ and σ represents the solution of the linear CD BFKL Eq. (3), while σ_{nl} stands for the solution of the non-linear CD BFKL Eq. (14). Therefore, our κ gives the strength of the non-linear effects with the non-perturbative corrections switched off

$$\kappa = \delta\sigma/\sigma = \frac{v(\xi)}{v(\xi) + 8\pi B} \sim$$
$$\sim 4\pi\kappa_c \frac{C_F}{\beta_0} \alpha_S(R_c/\sqrt{A})(e^{c\xi} - 1). \qquad (34)$$

The magnitude of non-linear effects is controlled, like in the case of small dipoles, by the ratio R_c^2/B (we assumed $R_c^2 \ll u/\Lambda^2$).

Numerical solution of Eqs. (3), (14) gives the r-dependence of $\kappa = \delta\sigma/\sigma$ shown in Fig. 2 for several values of x and for two correlation radii $R_c = 0.26$ and 0.52 Fm. For $\delta\sigma/\sigma \ll 1$ the law $\delta\sigma/\sigma \propto R_c^2/B$ holds true. At large $r \gtrsim R_c$ the toy-model solution, Eq. (29) (dashed lines) correctly reproduces the ξ-dependence of κ. At small $r \ll R_c$ the ratio $\delta\sigma/\sigma$ decreases slowly as it is prescribed by Eq. (23). In Fig. 2 also shown is the evolution of the unitarity ratio $\sigma_{nl}(\xi, r)/[4\pi(B_1 + B_2)]$ with $B_1 = B(\xi, R_c)$, $B_2 = B(\xi, r)$ and denoted by $\sigma/8\pi B$. High sensitivity of $\sigma_{nl}(\xi, r)$ to R_c is not surprising in view of the toy-model solution (29).

9. Summary. To summarize, the purpose of the present paper has been an exploration of the phenomenology of saturation in diffractive scattering which emerges from the BFKL dynamics with finite correlation length of perturbative gluons, R_c. The non-linear effects are shown to be dominated by the large size $q\bar{q} - g$ fluctuations of the probe (virtual gauge boson). They should very slowly, $\propto 1/\ln Q^2$, decrease at large Q^2. The magnitude of the non-linear effects is controlled by the dimensionless parameter $\kappa_c = R_c^2/8B$.
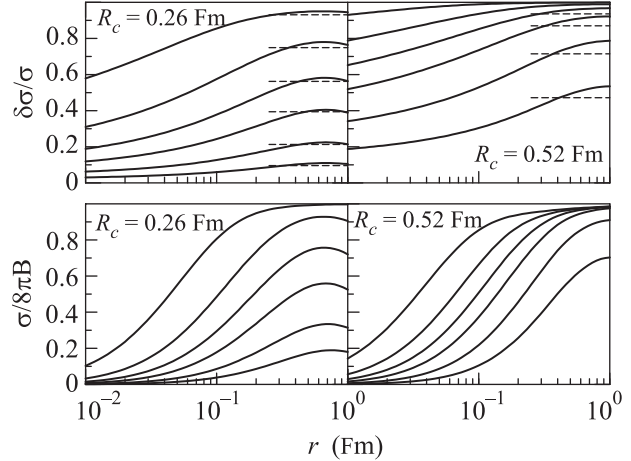

Fig. 2. The dipole size dependence of the non-linear correction $\kappa = \delta\sigma/\sigma$ to the linear CD BFKL dipole cross section σ for two correlation radii R_c and for $\xi = 6$, 8.5, 11, 13, 15.5, 20. Dashed lines correspond to the approximation $v(\xi) \approx \sigma_0(R_c^2)(e^{c\xi} - 1)$ in Eqs. (29), (30). Shown separately is the "unitarity ratio" $\sigma/8\pi B$ (see text) for two values of R_c and for the same set of ξ

The area populated with interacting gluons is proportional to the diffraction cone slope B. Smallness of κ_c makes the non-linear effects rather weak even at lowest Bjorken x available at HERA. The linear BFKL with the running coupling and the infrared regulator $R_c = 0.26$ Fm gives very good description of the proton structure function $F_2(x, Q^2)$ in a wide range of x and Q^2.

1. E. A. Kuraev, L. N. Lipatov and V. S. Fadin, Sov. Phys. JETP **44**, 443 (1976); **45**, 199 (1977); Ya. Ya. Balitskii and L. N. Lipatov, Sov. J. Nucl. Phys. **28**, 822 (1978).

2. O. V. Kancheli, Sov. Phys. JETP Lett. **18**, 274 (1973); Pisma Zh. Eksp. Teor. Fiz. **18**, 465 (1973).

3. N. N. Nikolaev and V. I. Zakharov, Phys. Lett. B **55**, 397 (1975); V. I. Zakharov and N. N. Nikolaev, Sov. J. Nucl. Phys. **21**, 227 (1975).

4. L. V. Gribov, E. M. Levin, and M. G. Ryskin, Phys. Rep. **100**, 1 (1983).

5. A. H. Mueller, J. Qiu, Nucl. Phys. B **268**, 427 (1986).

6. I. Balitsky, Nucl. Phys. B **463**, 99 (1996); Phys. Rev. D **60**, 014020 (1999).

7. Yu. V. Kovchegov, Phys. Rev. D **60**, 034008 (1999); Phys. Rev. D **61**, 074018 (2000).

8. M. Braun, Eur. Phys. J. C **16**, 337 (2000); Phys. Rev. D **61**, 074018 (2000).

9. N. N. Nikolaev and W. Schäfer, Phys. Rev. D **74**, 014023 (2006).

10. J. Bartels and K. Kutak, Eur. Phys. C **53**, 533 (2008).

11. E. Meggiolaro, Phys. Lett. B **451**, 414 (1999).

12. N. N. Nikolaev, B. G. Zakharov, and V. R. Zoller, JETP Lett. **59**, 6 (1994); Phys. Lett. B **328**, 486 (1994); JETP **78**, 806 (1994).

13. N. N. Nikolaev and B. G. Zakharov, J. Exp. Theor. Phys. **78**, 598 (1994); Z. Phys. C **64**, 631 (1994).

14. E. Witten, Nucl. Phys. B **160**, 67 (1979).

15. B. G. Zakharov, JETP Lett. **86**, 444 (2007).

16. A. H. Mueller, Nucl. Phys. B **415**, 373 (1994); A. H. Mueller and B. Patel, Nucl. Phys. B **425**, 471 (1994).

17. N. N. Nikolaev and B. G. Zakharov, Phys. Lett. B **327**, 149 (1994).

18. N. N. Nikolaev, B. G. Zakharov, and V. R. Zoller, JETP Lett. **66**, 138 (1997); N. N. Nikolaev, J. Speth, and V. R. Zoller, Phys. Lett. B **473**, 157 (2000).

19. N. N. Nikolaev, B. G. Zakharov, and V. R. Zoller, JETP Lett. **66**, 137 (1997).

20. J. Nemchik, N. N. Nikolaev, E. Predazzi et al., JETP **86**, 1054 (1998).

21. R. Fiore, N. N. Nikolaev, and V. R. Zoller, JETP Lett. **90**, 319 (2009); N. N. Nikolaev and V. R. Zoller, Phys. Atom. Nucl. **73**, 672 (2010).

22. J. Breitweg et al. (ZEUS Collaboration), Phys. Lett. B **407**, 432 (1997).

23. M. Derrick et al. (ZEUS Collaboration), Z. Phys. C **72**, 399 (1996).

24. C. Adloff et al. (H1 Collaboration), Nucl. Phys. B **497**, 3 (1996).

25. S. Aid et al. (H1 Collaboration), Nucl. Phys. B **470**, 3 (1996).

26. M. R. Adams et al. (E665 Collaboration), Phys. Rev. D **54**, 3006 (1996).

27. M. Glück, E. Reya, and A. Vogt, Eur. Phys. J. C **5**, 461 (1998).

28. R. Fiore and V. R. Zoller, JETP Lett. **95**, 55 (2012); Pisma v ZhETF **95**, 61 (2012); arXiv: 1107.4456 [hep-ph].

29. J. L. Albacete, N. Armesto, J. G. Milhano et al., Eur. Phys. J. C **71**, 1705 (2011); J. L. Albacete, N. Armesto, J. G. Milhano, and C. Salgado, Phys. Rev. D **80**, 034031 (2009).

30. N. N. Nikolaev, B. G. Zakharov, and V. R. Zoller, JETP Lett. **60**, 694 (1994).

31. N. N. Nikolaev, B. G. Zakharov, and V. R. Zoller, Phys. Lett. B **366**, 337 (1996).

32. R. Fiore and V. R. Zoller, *UHE Neutrinos: Fusing Gluons Within Diffraction Cone*, talk at *Low x meeting*, Santiago de Compostela, Spain, June 2 - 7, 2011; arXiv:1111.0516 [hep-ph].

33. K. Kutak and J. Kwiecinski, Eur. Phys. J. C **29**, 521 (2003).

34. J. Bartels, E. Gotsman, E. Levin, and U. Maor, Phys. Lett. B **556**, 114 (2003); Phys. Rev. D **68**, 054008 (2003).

35. I. P. Ivanov, N. N. Nikolaev, and A. A. Savin, Phys. Part. Nucl. **37**, 1 (2006).

36. V. N. Gribov and L. N. Lipatov, Sov. J. Nucl. Phys. **15**, 438 (1972); L. N. Lipatov, Sov. J. Nucl. Phys. **20**, 181 (1974); Yu. L. Dokshitzer, Sov. Phys. JETP **46**, 641 (1977); G. Altarelli and G. Parisi, Nucl. Phys. B **126**, 298 (1977).

37. J. Jalilian-Marian and Yu. V. Kovchegov, Prog. Part. Nucl. Phys. **56**, 104 (2006).

38. Yu. L. Dokshitzer, Sov. Phys. JETP **46**, 641 (1977).

39. N. N. Nikolaev, W. Schäfer, and G. Schwiete, Phys. Rev. D **63** 014020 (2000).

40. N. N. Nikolaev and B. G. Zakharov, Phys. Lett. B **332**, 177 (1994).

41. N. N. Nikolaev and B. G. Zakharov, Phys. Lett. B **332**, 184 (1994).